PAPER

Optimization of optical properties of photonic crystal fibers infiltrated with chloroform for supercontinuum generation

IOP Publishing | Astro Ltd Laser Physics

Laser Phys. **29** (2019) 075107 (9pp) https://doi.org/10.1088/1555-6611/ab2115

Optimization of optical properties of photonic crystal fibers infiltrated with chloroform for supercontinuum generation

Chu Van Lanh[1], Van Thuy Hoang[2,3], Van Cao Long[4], Krzysztof Borzycki[5], Khoa Dinh Xuan[1], Vu Tran Quoc[1], Marek Trippenbach[2], Ryszard Buczyński[2,3] and Jacek Pniewski[2]

[1] Department of Physics, Vinh University, 182 Le Duan, Nghe An Province, Vinh City, Viet Nam
[2] Faculty of Physics, University of Warsaw, Pasteura 5, 02-093 Warsaw, Poland
[3] Department of Glass, Institute of Electronic Materials Technology, Wólczyńska 133, 01-919 Warsaw, Poland
[4] Institute of Physics, University of Zielona Góra, Prof. Szafrana 4a, 65-516 Zielona Góra, Poland
[5] National Institute of Telecommunications, Szachowa 1, 04-894 Warsaw, Poland

E-mail: j.pniewski@uw.edu.pl

Received 8 January 2019
Accepted for publication 6 May 2019
Published 28 May 2019

Abstract

A photonic crystal fiber made of fused silica glass, infiltrated with chloroform ($CHCl_3$), is proposed as a new source of supercontinuum (SC) light. Guiding properties in terms of effective refractive index, attenuation, and dispersion of the fundamental mode are studied numerically. As a result, two optimized structures are selected for and verified against SC generation in detail. The dispersion characteristic of the first structure is all-normal and equals -7 ps $\cdot$ nm^{-1} $\cdot$ km^{-1} at 0.92 μm, while the dispersion characteristic of the second structure has the zero-dispersion wavelength at 1 μm, and SC generation was demonstrated for the wavelength 1.03 μm. We prove the possibility of coherent octave-wide SC generation in the wavelength range of 600–1260 nm and soliton fission based low-coherence flat SC in the wavelength range of 600–1400 nm, with 400 fs pulses and 0.8 nJ of energy in-coupled into the core of the studied structures. Proposed fibers are good candidates for all-fiber SC sources as an alternative to glass core fibers, since nonlinearity of $CHCl_3$ is higher than silica and its toxicity is negligible. The proposed solution may lead to new low-cost all-fiber optical systems.

Keywords: photonic crystal fibres (PCFs), chloroform, supercontinuum (SC) generation, dispersion, nonlinear optics

(Some figures may appear in colour only in the online journal)

1. Introduction

Since the invention of photonic crystal fibers (PCFs) in 1996 [1], their unique optical properties have been thoroughly analyzed. Among these properties one can find single-mode guidance [2, 3], possibility to tailor dispersion characteristics [4, 5] or birefringence [6]. New kinds of PCFs were also presented, such as large-mode area fibers [7] or all-solid fibers [8]. Several applications were proposed, including sensors [9], lasers [10] or novel supercontinuum-based light sources [11].

Original PCFs contained air-holes in the cladding and/or in the core, providing different guiding mechanisms. Such a static optical device cannot be easily tuned. Infiltration of PCFs with specific liquids or other materials adds an extra

degree of freedom that enlarges the possibility of application [12–14]. Further modification of guiding properties of the fibers on-the-fly are possible, when an external electric field is applied [15] or the temperature is changed [16].

A flat dispersion characteristic is crucial for efficient supercontinuum (SC) generation in both normal and anomalous dispersion regime. A careful choice of the internal structure of a PCF and the type of the liquid allows for an efficient SC generation. In most of the papers presenting SC in liquid-filled PCFs the ultrafast Kerr-nonlinearity of such liquids as carbon disulfide (CS_2), toluene (C_7H_8), carbon tetrachloride (CCl_4), ethanol (C_2H_5OH) or chloroform ($CHCl_3$) are exploited [17–28]. The liquids have the nonlinear refractive index n_2 higher than fused silica, even up to 200 times for CS_2, and are transparent in the visible and near infrared (NIR) wavelength range. However, because of high toxicity as well as explosive, carcinogenic and volatile properties of CS_2, other less dangerous liquids are preferred in practical applications.

Different concepts of the PCF structure and concept of filling only a part of the fiber were studied. Vieweg *et al* have shown a two-photon direct-laser writing technique that allows for closing of individual air-holes in a PCF and demonstrated SC generation in a PCF infiltrated with CCl_4, using femtosecond pump (210 fs-long pulses with a center wavelength of 1.03 μm). For the beam power of 100 mW a 600 nm-wide SC spectrum was obtained [17]. Later, a theoretical design of a liquid-filled PCF was also presented, where only one ring of holes surrounding the core was filled with a hypothetical liquid. It resulted in near zero ultra-flat dispersion, as small as 0 ± 0.41 ps/nm/km for a broad wavelength range and SC in the 400 nm-wide range, although given within the dynamics of 100 dB [18].

Numerical calculations and an experimental verification of the SC generation in a CS_2-filled 16 cm-long PCF were presented by Churin *et al*. The PCF was pumped with compact mode-locked fiber lasers pumping at 1.56 μm and 1.91 μm and the SC spanned the wavelength ranges 1.46–2.1 μm and 1.79–2.4 μm at 20 dB level [19]. Then, a SC generation in the mid-IR wavelength range in capillary fibers filled with CS_2 was also shown. This allowed for a spectral width of over 1.2 μm and 1 μm, at pump wavelengths of 1.03 μm, 1.51 μm, and 1.685 μm, and with 450 fs-long pulses [20]. Recently, a possibility of SC generation in a PCF with the central core filled with toluene was demonstrated. The spectral range of the SC was from 1.0 to 1.75 μm, for 450 fs-long pulses, 3 nJ pulse energy and pump wavelength 1.55 μm [21]. For ethanol a PCF of length 20 cm was presented, with the pump wavelength 1550 nm, pulse energy 4 nJ and pulse duration 80 fs. It can generate 945 nm of flattened broadband SC spectrum in the IR [22]. For carbon tetrachloride the possibility of coherent, octave-spanning SC generation with 300 fs pulses with only 0.8 nJ of energy in-coupled into the core was demonstrated [23].

More complicated theoretical PCFs were also proposed. They use two different liquids, namely C_7H_8 in the core and CCl_4, $CHCl_3$, C_2H_5OH, and H_2O in the first ring of holes surrounding the core. This allowed for spectral broadening as wide as 2 μm in both the visible and near-infrared regions, when a 50 fs input optical pulse of peak power 10 kW and center wavelength 1560 nm was launched into a 10 mm-long PCF [24]. Finally, a detailed analysis and experimental verification of hybrid soliton dynamics as an important mechanism of SC generation was presented by Chemnitz *et al*, for a capillary fiber filled with CS_2, pumped in the anomalous dispersion regime by a 460 fs laser operating at 1.95 μm. The authors have shown an octave-spanning SC in the range 1.1–2.7 μm at 14 nJ pulse energy [25]. Subsequently, soliton-fission mediated infrared SC generations in liquid-core capillary fibers using highly transparent carbon chlorides (CCl_4, C_2Cl_4) were presented that allowed for octave-spanning bandwidths (1.1 μm to 2.4 μm) in case of the core filled with C_2Cl_4. The broadening was reported for pulse energy as low as 0.5 nJ, using 270 fs-long pulses at 1.92 μm wavelength [26].

For $CHCl_3$, which is chloroform, two theoretical PCFs with liquid-filled cores were proposed up till now. The first one had zero dispersion wavelength (ZDW) at 763.6 nm. The pump wavelength was 800 nm, while the pulses lasted 120 fs with the repetition rate 76 MHz. The average power was 2 kW. The exact wavelength range and the degree of coherence of the SC it is not fully determined, but it can be estimated as approx. 550–1400 nm with 40 dB dynamics, achieved on 5 mm-long fiber [27]. The second one was modelled numerically in all-normal regime and for specific geometrical parameters. The dispersion in the vicinity of 1.06 μm pump wavelength was in the range from -20 to -50 ps/nm/km. As a result, a flat SC with high degree of coherence spanning near 2 octaves, from 340 nm to 1360 nm at 20 dB level was predicted, when 100 fs pulses were launched in the 0.01 m-long fiber (with 47 kW peak power) [28].

The nonlinear refractive index n_2 of $CHCl_3$ was 1.7×10^{-18} $m^2\,W^{-1}$ [26] or 6.17×10^{-19} $m^2\,W^{-1}$ [28]. It should be underlined that the [28] is based on the work by Ho and Alfano from 1979 [29], while most recently this value was estimated by Zhao *et al* at 1.64×10^{-19} with the accuracy of 20% for the case where all mechanisms of the nonlinear response are present. In their paper the dependence of n_2 on the pulse time was studied and they claim that it may lead to discrepancies between different papers [30]. Therefore, in particular, the result obtained by Wang *et al* may by inaccurate due to too high n_2 assumed by authors.

In present paper we propose and analyze a PCF made of fused silica glass, with $CHCl_3$-filled core, to be used as a NIR SC source pumped with low-energy pulses. Among common nonlinear liquids such as CS_2, CCl_4 and $CHCl_3$, the latter has the lowest material dispersions in the visible region. Near- and mid-infrared wavelength range seems convenient for applications in novel areas, such as quality and security control or environmental monitoring, since in this spectral region many substances exhibit strong resonances associated with the fundamental rotational and vibrational resonances of various technologically vital molecules [31].

Guiding properties of proposed fiber in terms of effective refractive index, attenuation and dispersion of the fundamental mode were studied. As a result two setups were selected and analyzed in detail. They allow for coherent and non-coherent SC. In our study we used Generalized Nonlinear Schrödinger Equation (GNLSE) to SC generation for both setups. The advantages of both these fibers are discussed at the end of the manuscript.

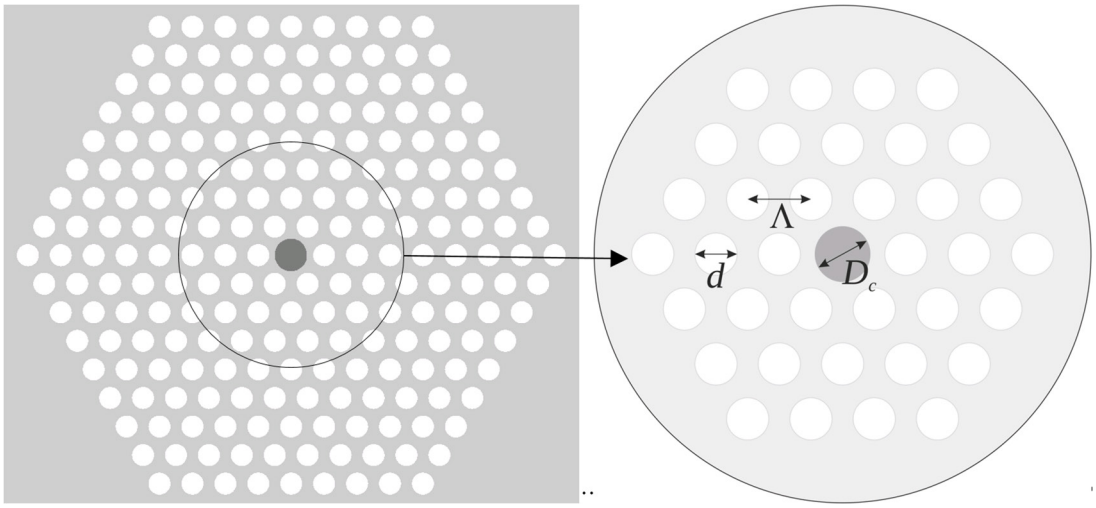

Figure 1. The schematic of the modelled PCF structure. Coefficient D_c is the diameter of the liquid-filled core.

2. Numerical modelling of the PCF

The schematic view of the geometrical structure of the modelled $CHCl_3$-filled PCF is shown in figure 1. It consists of 8 rings of air-holes ordered in a hexagonal lattice, surrounding the central liquid-filled hole. The linear filling factor of the cladding is defined as $f = d/\Lambda$, where d is the diameter of a single air-hole, and Λ is the lattice constant. We assume that PCF is made of fused silica glass (SCHOTT Lithosil®). The central hole is filled with $CHCl_3$. Chloroform is a colorless, transparent liquid, easy to evaporate, with heavy ethereal odor. Figure 2 depicts the characteristics of the real and imaginary part of the refractive index of $CHCl_3$ compared to fused silica glass. $CHCl_3$ is transparent in a broad range of visible and near infrared wavelengths, even though it has few absorption maxima, at 1.152 μm, 1.410 μm, and 1.691 μm. The highest peak at 1.691 μm reaches k value equal 2.65×10^{-4} what implies the attenuation a at this wavelength equal to 85.6 dB cm^{-1}, calculated from the relation below,

$$a = 10 \cdot \log\left[e^{(4\pi k/\lambda)}\right], \qquad (1)$$

where λ is the wavelength. Refractive index characteristics are modelled using Sellmeier's equation as given below, where the C_i coefficients have dimensions of micrometers squared (μm^2)

$$n^2(\lambda) = A_1 + \frac{B_1\lambda^2}{\lambda^2 - C_1} + \frac{B_2\lambda^2}{\lambda^2 - C_2} + \frac{B_3\lambda^2}{\lambda^2 - C_3}. \qquad (2)$$

The Sellmeier's coefficients for fused silica and $CHCl_3$ are presented in table 1.

3. Modelling modal and dispersion properties of the PCF

First, preliminary numerical simulations were conducted for the lattice constants equal 1.0 μm, 1.5 μm, 2.0 μm, and 2.5 μm and for the filling factors 0.3, 0.35, 0.4, 0.45, 0.5, 0.55, 0.6, 0.65, 0.7, 0.75, and 0.8. As a result 44 simulations were conducted at this stage. For each simulation run the diameter of the core was calculated from the equation $D_c = 2\Lambda - 1.1d$. The smallest core diameter was 1.12 μm for $\Lambda = 1.0$ μm and $f = 0.8$. The biggest core diameter was 4.175 μm for $\Lambda = 2.5$ μm and $f = 0.3$. A commercial-grade simulator, eigenmode solver and propagator was used to perform the calculations in case of modal and dispersion properties of the PCF [33], with the assumption that $CHCl_3$ exhibits negligible losses. This does not influence dispersion characteristics.

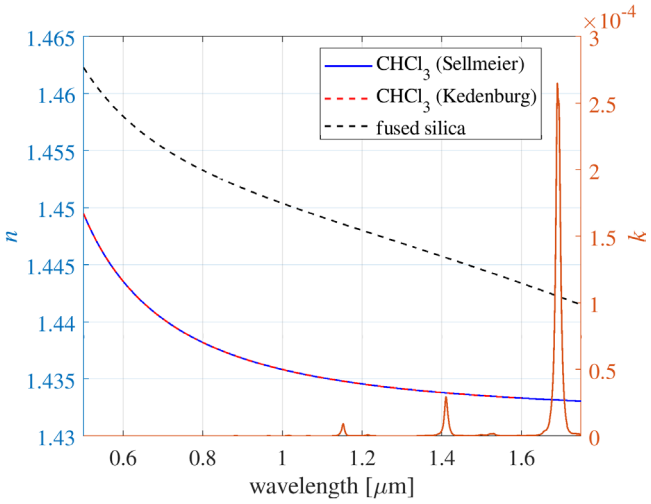

Figure 2. Characteristics of real (n) and imaginary (k) part of the refraction index of $CHCl_3$ for the temperature of 20 °C. The black dashed line denotes n of fused silica. The red dashed line is based on experimental data from [32], while the solid blue line is extrapolated using Sellmeier's equation.

The first ring of holes surrounding the core has the main influence on dispersion properties of the fiber, especially ZDW, while other rings are responsible for mode attenuation, especially for higher modes [34]. For the modeling we used a constant filling factor for all rings to simplify future fiber development. At this stage we do not verify if the selected fiber is a single-mode (SM) or multi-mode (MM) fiber. This analysis is performed for optimized fibers.

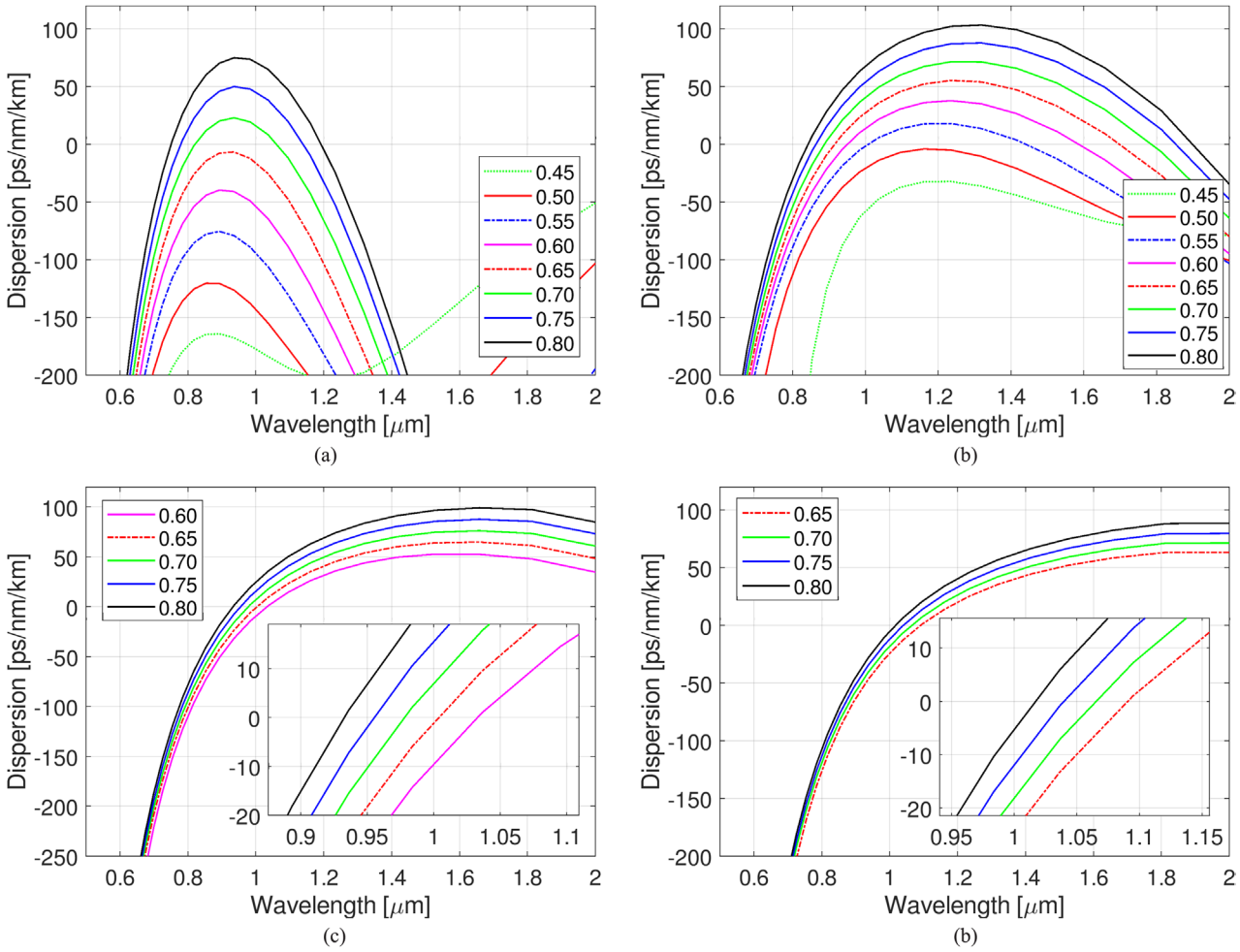

Figure 3. Characteristics of the PCF mode dispersion for filling factor f values in the range from 0.45 to 0.8 and lattice constants (a) 1.0 μm, (b) 1.5 μm, (c) 2.0 μm, and (d) 2.5 μm.

Table 1. Sellmeier's coefficients for the materials used.

Coefficient	Value
Fused silica	
B_1	0.669 4226
B_2	0.434 5839
B_3	0.871 6947
C_1	4.4801×10^{-3} μm^2
C_2	1.3285×10^{-2} μm^2
C_3	95.341 482 μm^2
$CHCl_3$	
B_1	1.046 47
B_2	0.003 45
C_1	0.010 48 μm^2
C_2	0.152 07 μm^2

In figures 3(a)–(d) characteristics of dispersion for the fundamental mode are shown for the wavelength range 0.5–2 μm. We have shown only those dispersion characteristics for which numerical solutions of the fundamental mode exist in the whole range of wavelengths. If f is getting small, the effective refractive index of the cladding is increasing according to the Maxell–Garnett theory of mixing, and exceeds the refractive index of the core, especially for large values of Λ. This results in nonexistence of modes located in the fiber's core.

On the basis of numerical simulations two fibers were selected, namely $\#F_1$ and $\#F_2$. The fiber $\#F_1$ is intended to generate coherent supercontinuum in the normal dispersion regime while pumped at 1030 nm. Therefore, we selected the geometrical parameters $\Lambda = 1.0$ μm and $f = 0.65$ since this fiber has all-normal dispersion and the maximum dispersion located at the wavelength 0.92 μm equals $-7\,\text{ps}\cdot\text{nm}^{-1}\cdot\text{km}^{-1}$. At the pump wavelength the dispersion equals $-24\,\text{ps}\cdot\text{nm}^{-1}\cdot\text{km}^{-1}$. One can also find another dispersion characteristics with $\Lambda = 1.0$ μm and $f = 0.5$ that exhibit better flatness of the dispersion in the all-normal regime but we were not able to obtain a coherent supercontinuum for this case.

The fiber $\#F_2$ is expected to generate supercontinuum of low coherence in the anomalous regime at the same pump wavelength as $\#F_1$, therefore we selected the geometrical parameters $\Lambda = 2.0$ μm and $f = 0.65$ since this fiber has ZDW at 1.0 μm and the dispersion at the pump wavelength equals $7.6\,\text{ps}\cdot\text{nm}^{-1}\cdot\text{km}^{-1}$, which is the lowest value for all dispersion characteristics with $\Lambda = 2.0$ μm. Figure 4 depicts the dispersion characteristics for these two fibers. The effective nonlinear coefficients γ for the fibers $\#F_1$ and $\#F_2$ are 1290

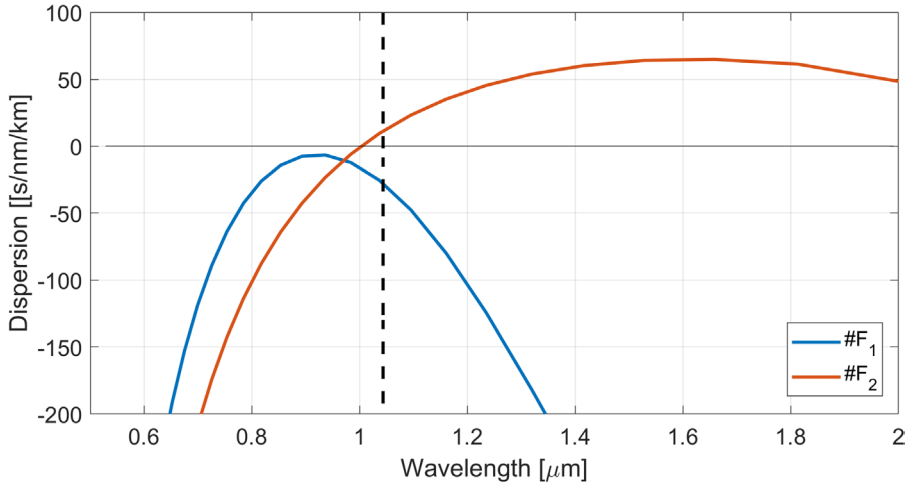

Figure 4. Characteristics of PCF mode dispersion for fibers #F_1 and #F_2. The dotted line indicates the pump wavelength 1030 nm.

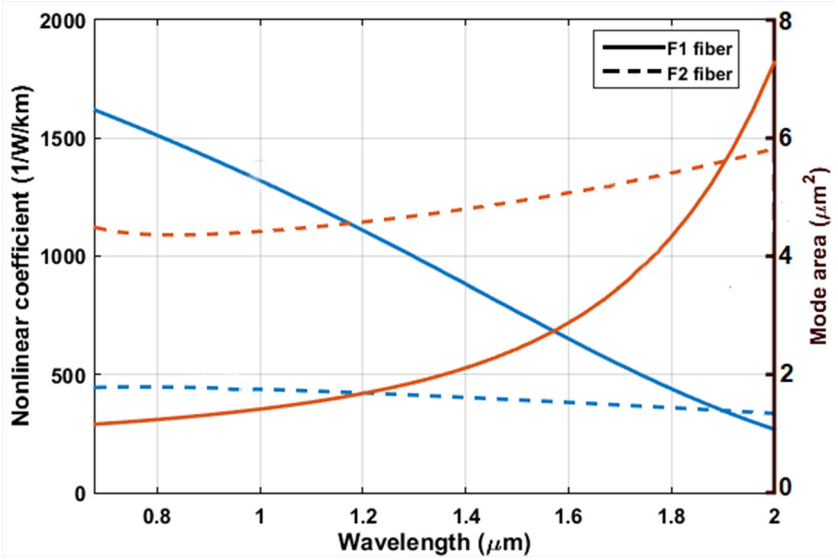

Figure 5. The effective nonlinear coefficient γ and the mode area of #F_1 and #F_2 fibers. The blue lines depicts nonlinear coefficient, while the red ones—the mode area.

$W^{-1} \cdot km^{-1}$ and 440 $W^{-1} \cdot km^{-1}$ for preferable pump wavelength of 1030 nm, while their effective mode areas are 1.5 μm^2 and 4.48 μm^2, respectively (see figure 5). The coefficient γ is calculated from the equation $\gamma = n_2\omega_0/cA_{eff}$, where ω_0 is the central frequency of the pulse, c is the speed of light in vacuum and A_{eff} is the effective mode area of the fiber. Both structures are effectively single-mode since any other mode has attenuation two orders of magnitude higher than the fundamental mode or is located in the cladding.

4. Supercontinuum generation in selected fibers

The nonlinear properties of the investigated fibers are calculated numerically solving the generalized nonlinear Schrödinger equation (GNLSE) using split-step Fourier method (SSFM) [35]

$$\partial_z \widetilde{A} = i\widetilde{\beta}(\omega)\widetilde{A} - \frac{\widetilde{\alpha}(\omega)}{2}\widetilde{A} + i\frac{n_2(\omega_0)\omega}{cA_{eff}(\omega)}\widetilde{A}\mathcal{F}\left[\int_{-\infty}^{\infty} R(t')|A|^2(t-t')\,dt'\right], \quad (3)$$

Table 2. Nonlinear parameters used in simulations [30]. The subscripts *el*, *d*, *l*, *c* indicate the following mechanisms: the bound-electronic, molecular reorientation, molecular interaction and collision-induced, respectively.

Parameter	Value
$n_{2,el}$	$0.41 \cdot 10^{-19}$ m^2 W^{-1}
$n_{2,d}$	$0.75 \cdot 10^{-19}$ m^2 W^{-1}
$\tau_{r,d}$	0.25 ps
$\tau_{f,d}$	1.8 ps
$n_{2,l}$	$0.4 \cdot 10^{-19}$ m^2 W^{-1}
$n_{2,c}$	$0.08 \cdot 10^{-19}$ m^2 W^{-1}
$\tau_{r,c}$	0.1 ps
$\tau_{f,c}$	0.1 ps

where $\widetilde{A}(\omega)$ is the frequency domain of an envelope pulse $A(t)$. The influence of the dispersion characteristic $\beta(\omega)$ on the nonlinear properties of the fiber are described by a product of the complex spectral envelope $\widetilde{A}(\omega)$ and

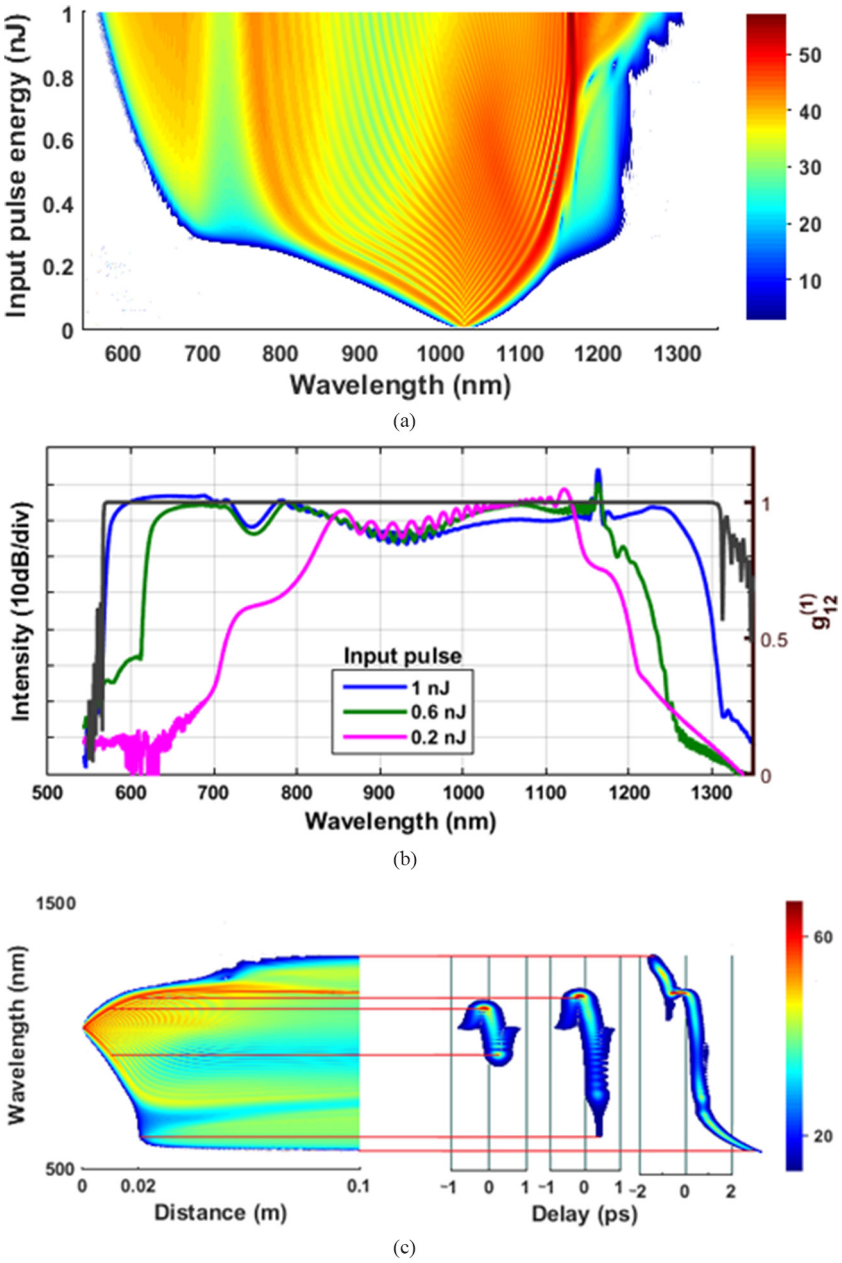

Figure 6. (a) SC spectrum calculated at a distance of 10 cm of the fiber #F_1 pumped with pulses of 400 fs duration, 1030 nm pump wavelength, and different pulse energy (b) supercontinuum spectrum estimated for 10 cm length of the fiber pumped with pulses of 400 fs duration, 1030 nm pump wavelength, various pulse energy and degree of coherence calculated from 20 individual pairs with random noise for 1 nJ input pulse energy (c) evolution along the fiber of the SC spectrum for the input pulse energy of 1 nJ.

$\widetilde{\beta}(\omega) = \beta(\omega) - (\omega - \omega_0)\beta_1 - \beta_0$. The term $\widetilde{\alpha}(\omega)$ is the frequency domain of attenuation coefficient $\alpha(t)$. In the simulations, the attenuation term is approximated by the sum of confinement and material loss. The nonlinear response function $R(t')$ is a sum of all contributing mechanisms listed by Zhao *et al* [30]. The nonlinear coefficient includes the nonlinear refractive index n_2 of $CHCl_3$ and the effective mode area A_{eff}. Table 2 presents the values of all respective parameters.

Coherence characteristics of fibers investigated in our model take into account shot noise and spontaneous Raman scattering. Because the first-order coherence has a more straightforward interpretation in terms of classical optics, it will be used to discuss noise-related issues. The coherence characteristics are calculated numerically using equation (4) [36] for ensembles of the corresponding supercontinuum spectra

$$\left|g_{12}^{(1)}(\lambda, t_1 - t_2 = 0)\right| = \left|\frac{\langle E_1^*(\lambda,t)\,E_2(\lambda,t)\rangle}{\left[\left\langle|E_1(\lambda,t)|^2\right\rangle\left\langle|E_2(\lambda,t)|^2\right\rangle\right]^{1/2}}\right|. \quad (4)$$

The pulses have the central wavelength 1030 nm and the duration 400 fs. The evolution of supercontinuum is simulated over a propagation distance of 10 cm with various input pulse energy in the range of $0 \div 1$ nJ, which corresponds to the peak power in the range of 0–4.16 kW. Particularly, in case of the

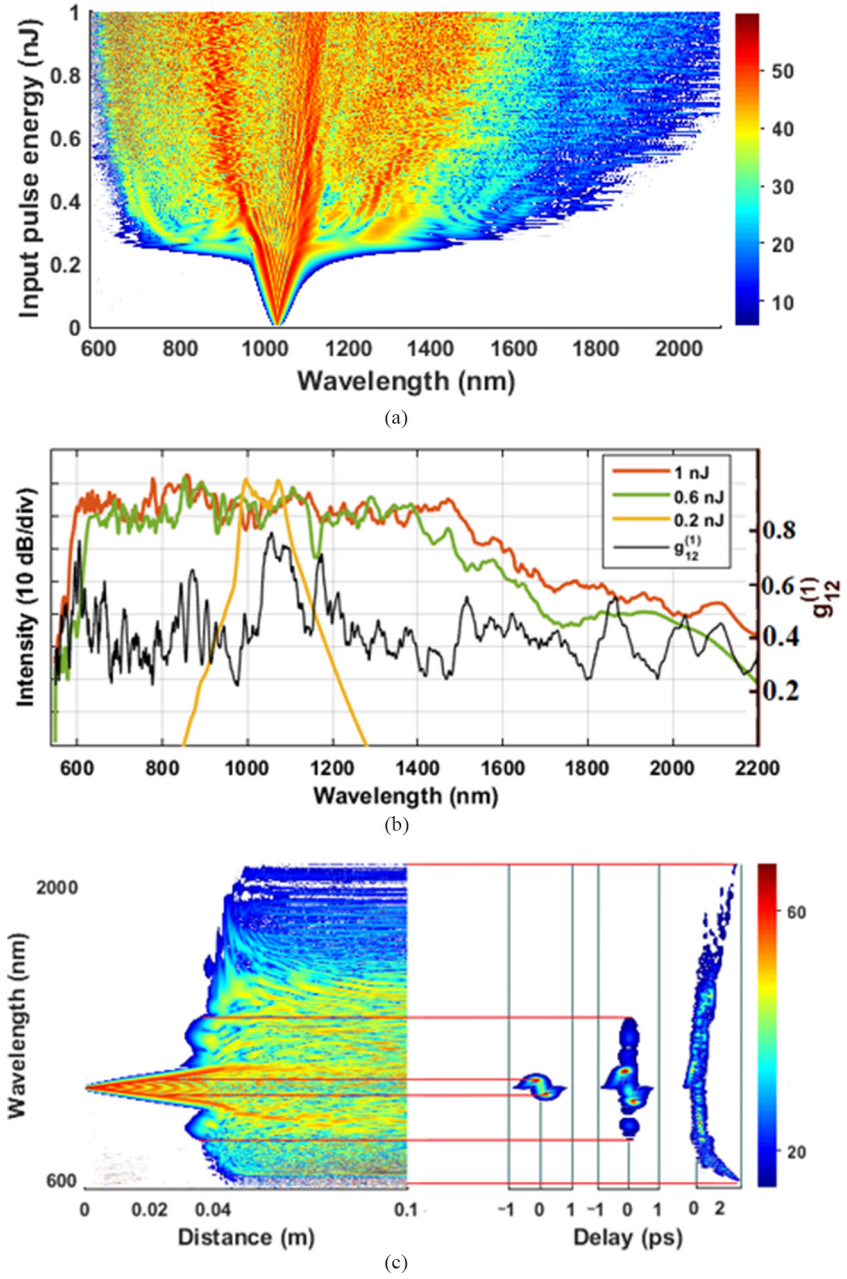

Figure 7. (a) SC spectrum calculated at a distance of 10 cm of the fiber $\#F_2$ when pumped with pulses of 400 fs duration, 1030 nm pump wavelength, and different pulse energy (b) supercontinuum spectrum estimated for 10 cm length of the fiber when pumped with pulses of 400 fs duration, 1030 nm pump wavelength, various pulse energy and degree of coherence calculated from 20 individual pairs with random noise for 1 nJ input pulse energy (c) evolution along the fiber of the SC spectrum for the input pulse energy of 1 nJ.

input pulse energy 1 nJ, the spectrum would be investigated at various specific values of fiber length to clarify the contribution of nonlinear phenomena to spectral emission.

Since the fiber $\#F_1$ operates in the all-normal dispersion regime, the main phenomena contributing to SC are self-phase modulation (SPM) followed by optical wave breaking (OWB) (see figure 6). For the input pulse energy lower than 0.2 nJ SPM is the main contribution to the broadening of the spectrum. The most remarkable feature is the symmetric shape of the incident pulse and the development of an oscillatory structure in the spectrum. The spectrum consist of many peaks and the outermost peaks are the most intense. In the case of low input pulse energy, below 0.2 nJ, the obtained broadening is very limited since only SPM process occurs (figure 6(a)). The optical wave breaking (OWB) begins to show up when the input pulse energy is higher than 0.2 nJ, which corresponds to 0.83 kW of peak power. This leads to the broadening at the blueshifted (trailing) edge and redshifted (leading) edge of the pulse, as shown in figure 6(a). Figure 6(b) depicts the degree of coherence calculated from 20 individual pairs of spectra generated with the random initial noise seed (single photon per mode noise model was used in the simulations). In the SC range high degree of coherence is maintained. Coherence of the long-wavelength range is limited to 1300 nm, however this is a result of low intensity and limit of spectra broadening related to high negative dispersion and steep dispersion curve

at this range (figure 4). Figure 6(c) shows the evolution of the SC spectrum along the fiber structure, and pulse spectrograms at three different locations along the propagation length.

During the initial propagation in the fiber the spectral broadening is dominated by SPM. The central section exhibits an almost linear chirp, i.e. the instantaneous frequency varies linearly in time. It leads to the typical S-shape of the spectrogram. For the input pulse energy 1 nJ OWB begins creating new wavelengths at 2 cm at the trailing edge around 550 nm because the initial SPM-induced broadening occurred slightly asymmetric towards the short wavelengths. On the leading edge OWB occurs only after 6 cm with a new wavelength band generated at around 1250 nm. Steep dispersion and decreasing nonlinear feature at long-wave limit lead to the suppression of the broadening of spectra. During further propagation, the energy would be redistributed from central frequency to the spectral wings, so temporal spectra become smooth, continuous and flat.

In the case of the $\#F_2$ fiber simulations, SPM is also the dominant mechanism for broadening of the spectrum when input pulse energy is smaller than 0.2 nJ. When pulse energy is higher than 0.2 nJ, the spectrum is broadened by subsequent soliton fission (SF) and by soliton self-frequency shift (SSFS) accompanied by the dispersive wave generation and four-wave mixing (FWM) (figure 7(a)). The complex degree of first-order coherence is calculated from 20 individual pairs of spectra generated with the random noise seed and shown in figure 7(b). The coherence of the SC is low since the modulation instability frequency components are not coherent with the pump and fission of each soliton occurs randomly, so fission products are completely incoherent.

For the fiber $\#F_2$ if the input pulse energy is 1 nJ, the dispersion length L_D is 12.8 m, and at the highest peak power the nonlinear length L_{NL} is 0.55 mm. Thus, the soliton number $N = (L_D/L_{NL})^{1/2}$ is approx. 152 and the soliton fission length is 8.4 cm. The idler terms began to appear at the 3.5 cm of propagation and then it is supported by four-wave mixing, which is the main contribution to spectrum broadening of SC generation before SF occurred, as shown in figure 7(c). After SF, the spectrum would be influenced by SSFS at leading edge and the dispersive wave (across the ZDW) at the trailing edge.

5. Conclusions

Of many highly nonlinear liquids chloroform is the one that combines several interesting properties, which make it a good candidate as nonlinear medium for use in highly nonlinear liquid-core PCFs. The nonlinearity of $CHCl_3$ ($n_2 = 1.64 \times 10^{-19}$) is one order of magnitude higher than of fused silica ($n_2 = 2.74 \times 10^{-20}$ m^2 W^{-1}) and is comparable to CCl_4 (1.53×10^{-19} m^2 W^{-1}), but at the same time it is significantly lower than of toluene ($n_2 = 16 \times 10^{-19}$ m^2 W^{-1}) and CS_2 ($n_2 = (4.3–5.1) \times 10^{-18}$ m^2 W^{-1}). The advantage of $CHCl_3$ is its negligible toxicity when compared to CS_2 and toluene. In our opinion it is extremely important for practical applications. Finally, linear refractive index of $CHCl_3$ is only about 0.012 lower than silica one. The latter allows for easy design of effectively single mode silica PCFs infiltrated with chloroform with a core size similar to standard silica fibers.

We have optimized the geometrical parameters of the PCFs with a chloroform-filled core to obtain both all-normal and anomalous dispersion characteristics. The proposed PCFs have high effective nonlinear coefficient of 1290 W^{-1} · km^{-1} and 440 W^{-1} · km^{-1} for the fibers $\#F_1$ and $\#F_2$, respectively, while relatively large mode is maintained.

The PCF parameters allow for high coupling efficiency with standard femtosecond fibers and high fiber nonlinearity. With the moderate input pulse energy of 1 nJ and the pulse duration 400 fs it is possible to obtain SC with low-cost commercial femtosecond fiber lasers emitting at 1030 nm. For the $\#F_1$ fiber an octave-wide all-normal supercontinuum generation in the range of 600–1260 nm can be achieved. A soliton fission based low-coherence flat SC in the range of 600–1400 nm can be generated in the $\#F_2$ fiber. The nonlinear processes occurring during SC generation in normal and anomalous regimes are similar to the ones that exist in other previously reported PCFs with cores filled with highly nonlinear liquids as toluene, carbon tetrachloride or carbon disulfide [21, 23, 25].

Both proposed fibers are good candidates for all-fiber SC sources as an alternative to glass core fibers, since nonlinearity of $CHCl_3$ is higher than silica and its toxicity is negligible. They allow for SC generation on the basis of two mechanisms, with different properties. The first one is SC in all-normal dispersion regime, that can be coherent. To our knowledge this solution is not currently available on the market. The second one is soliton fission—based SC in anomalous regime of dispersion. Moreover, in our solution pulse power as low as 1 nJ is required for SC in the broad range of wavelengths due to high nonlinearity of chloroform. The all-fiber systems are robust, shock-proof and do not need axis adjustment or additional pulse compressors. However, before they can become really useful, the issues related to fusion splicing of liquid core PCFs and standard silica fibers should be solved. This concern is still under investigation and different modifications of fusion splicing methods are proposed up to now [37, 38].

Acknowledgments

Narodowe Centrum Nauki (NCN) (UMO-2016/21/M/ST2/00261); Foundation for Polish Science (FNP) (TEAM TECH/2016-1/1) Team Programme co-financed by the European Regional Development Fund under Smart Growth Operational Programme (SG OP), Priority Axis IV; H2020 ACTPHAST 4.0 (Grant No. 779472); Vietnam's Ministry of Education and Training (B2017-TDV-03); Uniwersytet Warszawski (UW) (statutory research).

References

[1] Knight J C, Birks T A, Russell P S J and Atkin D M 1996 All-silica single-mode optical fiber with photonic crystal cladding *Opt. Lett.* **21** 1547–9

[2] Birks T A, Knight J C and Russell P S J 1997 Endlessly single-mode photonic crystal fiber *Opt. Lett.* **22** 961–3

[3] Cregan R F, Mangan B J, Knight J C, Birks T A, Russell P S J, Roberts P J and Allan D C 1999 Single-mode photonic band gap guidance of light in air *Science* **285** 1537–9

[4] Knight J C, Arriaga J, Birks T A, Ortigosa-Blanch A, Wadsworth W J and Russell P S J 2000 Anomalous dispersion in photonic crystal fiber *Photon. Technol. Lett.* **12** 807–9

[5] Dabas B and Sinha R K 2010 Dispersion characteristic of hexagonal and square lattice chalcogenide As_2Se_3 glass photonic crystal fiber *Opt. Commun.* **283** 1331–7

[6] Ortigosa-Blanch A, Knight J C, Wadsworth W J, Arriaga J, Mangan B J, Birks T A and Russell P S J 2000 Highly birefringent photonic crystal fibers *Opt. Lett.* **25** 1325–7

[7] Baggett J, Monro T, Furusawa K and Richardson D 2001 Comparative study of large-mode holey and conventional fibers *Opt. Lett.* **26** 1045–7

[8] Luan F, George A K, Hedley T D, Pearce G J, Bird D M, Knight J C and Russell P S J 2004 All-solid photonic band-gap fiber *Opt. Lett.* **29** 2369–71

[9] Tuchin V V, Skibina Y S, Beloglazov V I, Chainikov M V, Skibina N B, Mikhailova N A, Zhestkov P M and Silokhin I Y 2008 Sensor properties of hollow-core photonic crystal fibers *Tech. Phys. Lett.* **34** 663–5

[10] Chen Z-H, Yang F, Chen D-J and Cai H-W 2017 A frequency-stabilized laser based on a hollow-core photonic crystal fiber CO_2 gas cell and its application scheme *Laser Phys.* **27** 045102

[11] Buczynski R, Pysz D, Stepien R, Waddie A J, Kujawa I, Kasztelanic R, Franczyk M and Taghizadeh M R 2011 Supercontinuum generation in photonic crystal fibers with nanoporous core made of soft glass *Laser Phys. Lett.* **8** 443–8

[12] Schmidt M A, Prill Sempere L N, Tyagi H K, Poulton C G and Russell P S J 2008 Waveguiding and plasmon resonances in two-dimensional photonic lattices of gold and silver nanowires *Phys. Rev.* B **77** 033417

[13] Ebnali-Heidari M, Dehghan F, Saghaei H, Koohi-Kamali F and Moravvej-Farshi M K 2012 Dispersion engineering of photonic crystal fibers by means of fluidic infiltration *J. Mod. Opt.* **59** 1384–90

[14] Pniewski J, Stefaniuk T, Le Van H, Long V C, Van L C, Kasztelanic R, Stepniewski G, Ramaniuk A, Trippenbach M and Buczynski R 2016 Dispersion engineering in nonlinear soft glass photonic crystal fibers infiltrated with liquids *Appl. Opt.* **55** 5033–40

[15] Du F, Lu Y Q and Wu S T 2004 Electrically tunable liquid-crystal photonic crystal fiber *Appl. Phys. Lett.* **85** 2181–3

[16] Van H L, Buczynski R, Long V C, Trippenbach M, Borzycki K, Manh A N and Kasztelanic R 2018 Measurement of temperature and concentration influence on the dispersion of fused silica glass photonic crystal fiber infiltrated with water–ethanol mixture *Opt. Commun.* **407** 417–22

[17] Vieweg M, Gissibl T, Pricking S, Kuhlmey B T, Wu D C, Eggleton B J and Giessen H 2010 Ultrafast nonlinear optofluidics in selectively liquid-filled photonic crystal fibers *Opt. Express* **18** 25232–40

[18] Maji P S and Chaudhuri P R 2014 Supercontinuum generation in ultra-flat near zero dispersion PCF with selective liquid infiltration *Optik* **125** 5986–92

[19] Churin D, Nguyen T N, Kieu K, Norwood R A and Peyghambarian N 2013 Mid-IR supercontinuum generation in an integrated liquid-core optical fiber filled with CS_2 *Opt. Mater. Express* **3** 1358–64

[20] Kedenburg S, Gissibl T, Steinle T, Steinmann A and Giessen H 2015 Towards integration of a liquid-filled fiber capillary for supercontinuum generation in the 1.2–2.4 μm range *Opt. Express* **23** 8281–9

[21] Lanh V C, Anuszkiewicz A, Ramaniuk A, Kasztelanic R, Dinh K X, Trippenbach M and Buczynski R 2017 Supercontinuum generation in photonic crystal fibres with core filled with toluene *J. Opt.* **19** 125604

[22] Van Le H, Cao V L, Nguyen H T, Nguyen A M, Buczynski R and Kasztelanic R 2018 Application of ethanol infiltration for ultra-flattened normal dispersion in fused silica photonic crystal fibers *Laser Phys.* **28** 115106

[23] Ho Dinh Q, Pniewski J, Le Van H, Ramaniuk A, Long V C, Borzycki K, Xuan K D, Klimczak M and Buczynski R 2018 Optimization of optical properties of photonic crystal fibers infiltrated with carbon tetrachloride for supercontinuum generation with subnanojoule femtosecond pulses *Appl. Opt.* **57** 3738–46

[24] Rael R, Ebnali-Heidari M and Saghaei H 2018 Supercontinuum generation in organic liquid–liquid core-cladding photonic crystal fiber in visible and near-infrared regions *JOSA* B **35** 323–30

[25] Chemnitz M, Gebhardt M, Gaida C, Stutzki F, Kobelke J, Limpert J, Tünnermann A and Schmidt M A 2017 Hybrid soliton dynamics in liquid-core fibres *Nat. Commun.* **8** 42

[26] Chemnitz M, Gaida C, Gebhardt M, Stutzki F, Kobelke J, Tünnermann A, Limpert J and Schmidt M A 2018 Carbon chloride-core fibers for soliton mediated supercontinuum generation *Opt. Express* **26** 3221–35

[27] Zhang H, Chang S, Yuan J and Huang D 2010 Supercontinuum generation in chloroform-filled photonic crystal fibers *Optik* **121** 783–7

[28] Wang C-C, Li W-M, Li N and Wang W-Q 2017 Numerical simulation of coherent visible-to-near-infrared supercontinuum generation in the $CHCl_3$-filled photonic crystal fiber with 1.06 μm pump pulses *Opt. Laser Technol.* **88** 215–21

[29] Ho P P and Alfano R R 1979 Optical Kerr effect in liquids *Phys. Rev.* A **20** 2170–87

[30] Zhao P, Reichert M, Benis S, Hagan D J and Stryland E W V 2018 Temporal and polarization dependence of the nonlinear optical response of solvents *Optica* **5** 583–94

[31] Willer U, Saraji M, Khorsandi A, Geiser P and Schade W 2006 Near- and mid-infrared laser monitoring of industrial processes, environment and security applications *Opt. Laser Eng.* **44** 699–710

[32] Kedenburg S, Vieweg M, Gissibl T and Giessen H 2012 Linear refractive index and absorption measurements of nonlinear optical liquids in the visible and near-infrared spectral region *Opt. Mater. Express* **2** 1588–611

[33] Lumerical Inc. (https://www.lumerical.com/products/)

[34] Saitoh K, Koshiba M, Hasegawa T and Sasaoka E 2003 Chromatic dispersion control in photonic crystal fibers: application to ultra-flattened dispersion *Opt. Express* **11** 843–52

[35] Dudley J M, Genty G and Coen S 2006 Supercontinuum generation in photonic crystal fiber *Rev. Mod. Phys.* **78** 1135–84

[36] Dudley J M and Coen S 2002 Coherence properties of supercontinuum spectra generated in photonic crystal and tapered optical fibers *Opt. Lett.* **27** 1180–2

[37] Kieu K, Schneebeli L, Norwood R A and Peyghambarian N 2012 Integrated liquid-core optical fibers for ultraefficient nonlinear liquid photonics *Opt. Express* **20** 8148–54

[38] Wang W, Yin X, Wu J, Geng Y, Tan X, Yu Y, Hong X, Du Y and Li X 2016 Realization of all-in-fiber liquid-core microstructured optical fiber *IEEE Photon. Technol. Lett.* **28** 609–12